Machine Copy for Proofreading, Vol. x, y–z, 2014

Analysis of Effect of Korean Offshore Wind Farms on Accuracy of X-band Tracking Radar

Joo-Ho Jung[1], In-O Choi[1], Kyung-Tae Kim[1], and Sang-Hong Park[2, *]

Abstract—Many government-led wind farms are being constructed in Korea as sources of clean and renewable energy. However, construction of these wind farms is continuously opposed by nearby military bases that operate X-band tracking radar because the amplitude and the phase of the electromagnetic waves reflected from the wind turbines may interfere with tracking radars installed along the coastline of the Korean peninsula. This paper proposes a method to analyze the effect of a wind farm on tracking radar, and presents the results of using the radar cross section of the blade of a real turbine predicted by the method of physical optics. Simulation results using various flight scenarios demonstrate that the tracking accuracy may be considerably degraded; thus appropriate action is required to eliminate this effect.

1. INTRODUCTION

The Korean government is pushing forward with many clean energy projects such as hydroelectric, nuclear, solar, and wind power generation, to mitigate Korea's shortage of natural petroleum deposits. Among these methods, wind power is the most promising because of the advanced construction technology of Korea, and therefore many wind farms are being constructed along its coast.

However, construction of the wind farm causes numerous objections because electromagnetic waves reflected from the wind turbine may seriously interfere with the X-band tracking radars located in nearby military bases. The large amplitude of the electromagnetic wave caused by the large radar cross section (RCS) [1, 2] of the wind turbine may distort the tracking radar signals and cause amplitude-comparison tracking radar (ACTR) to lock onto the large RCS of a wind turbine rather than onto the small RCS of an intended (possibly military) target (Fig. 1). Furthermore, the phase of the reflected signal can break the coherency of the radar signal and thus cause phase comparison tracking radar (PCTR) to fail at tracking objects. Therefore, to balance successful construction of wind farms and protection of Korean territory, analysis of the effects of wind farms on tracking radar is required.

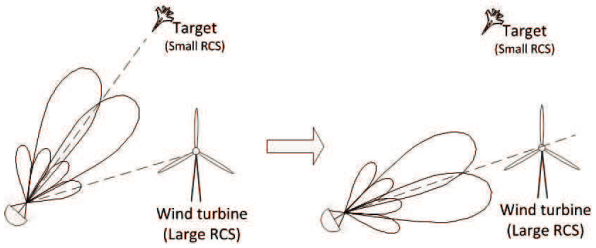

Figure 1. Failure by radar to tracking a target due to large signal from wind turbine.

Received 14 April 2014
* Corresponding author: Sang-Hong Park (radar@pknu.ac.kr).
[1] Department of Electrical Engineering, Pohang University of Science and Technology, Pohang, Gyungbuk, Korea. [2] Department of Electronic Engineering, Pukyong National University, Busan, Korea.

This paper proposes a method to analyze the effect of a wind farm on the results of ACTR and PCTR. The wind turbine analyzed was constructed by a representative Korean wind turbine maker, Hyundai Construction (www.hdec.kr). For accurate analysis, the mono-pulse radar signal for the two types of tracking radar was constructed by using RCS of the blade of the wind turbine predicted by the method of physical optics (PO), and various tracking tests were conducted in which single and multiple wind turbines existed in one antenna beam and target objects flew in various patterns. Then, the distance error and the probability of hitting the target, i.e., probability of kill (PK), with and without the wind turbine were compared and analyzed. In addition, the Doppler frequency caused by the multiple turbines was analyzed.

Analysis results demonstrate that wind turbines caused PK by PCTR to decrease by $> 20\%$ because of the large error in estimated distance to the target, and that they caused enormous errors by ACTR because it locked onto the wind turbine. The Doppler analysis obtained a maximum Doppler frequency that corresponds to the velocity of helicopter. Therefore, to avoid radar tracking errors caused by wind turbines, appropriate solutions such as data sharing among several radars, advanced radars and signal processing technique are required.

2. PRINCIPLES

2.1. Principle of Tracking Radar

In this paper, we analyzed ACTR and PCTR, two representative types of tracking radar that are widely used for surveillance [3]. ACTR utilizes four beams A, B, C, and D, each radiated by one of four antennas (Fig. 2) and the radar continuously compares the amplitude of each beam. When a target is on the tracking axis, i.e., tracked accurately, the four antennas receive equal energy [3]. However, when the target is off the tracking axis, the antennas receive differing amounts of energy (Fig. 3); to track the target, the radar system exploits information about the energy imbalance among the antennas to adjust its direction so that equal energy is collected by all of them (implementation explained below).

PCTR is similar to the ACTR except that it utilizes the phase instead of the amplitude. In this paper, we utilize the well-summarized principle given in [3]. We consider the case in which the target is off the tracking axis (Fig. 4). Using the cosine formula, the angular displacement of the radar is

$$R_1^2 = R^2 + \left(\frac{d}{2}\right)^2 - 2\frac{d}{2}R\cos\left(\varphi + \frac{\pi}{2}\right) = R^2 + \frac{d^2}{4} + dR\sin\varphi. \tag{1}$$

Assuming $d \ll R$, (1) can be approximated by the Taylor series:

$$R_1 \approx R\left(1 + \frac{d}{2R}\sin\varphi\right). \tag{2}$$

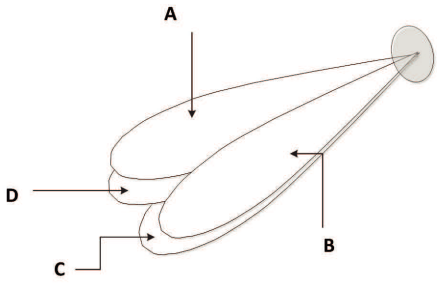

Figure 2. Four antennas used for ACTR.

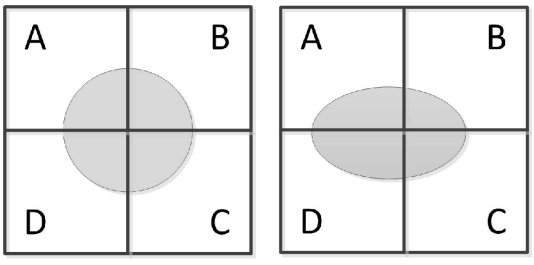

Figure 3. Antenna power received for two cases; area of the shaded region is the amount of energy received by each antenna. (a) On tracking axis. (b) Off tracking axis

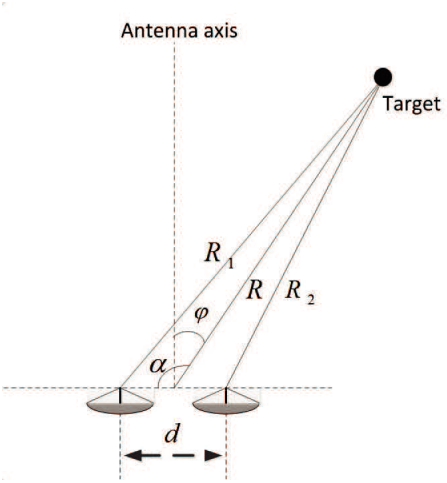

Figure 4. Observation scenario of PCTR.

Similarly,

$$R_2 \approx R\left(1 - \frac{d}{2R}\sin\varphi\right). \tag{3}$$

Thus, the phase difference caused the target is

$$\phi = \frac{2\pi}{\lambda}(R_1 - R_2) = \frac{2\pi}{\lambda}d\sin\varphi, \tag{4}$$

where λ is the wavelength of the operating signal. The radar illuminates so as to remove the phase error. However, measuring the phase error correctly is a difficult task, so sum (Σ) and difference (Δ) signals are used. Assuming radar signals S_1 and $S_2 = S_1 e^{-j\phi}$ received by the two elements 1 and 2, respectively, the signals received at the sum and the difference channels are [3]

$$\Sigma(\varphi) = S_2\left(1 - e^{j\phi}\right), \quad \Delta(\varphi) = S_2\left(1 + e^{-j\phi}\right). \tag{5}$$

Then, the phase error can be calculated from the ratio of the two channels as [3]:

$$\frac{\Delta}{\Sigma} = \frac{1 - e^{-j\phi}}{1 + e^{-j\phi}} = j\tan\left(\frac{\phi}{2}\right) \Rightarrow \phi = 2\tan^{-1}\left(\frac{|\Delta|}{|\Sigma|}\right). \tag{6}$$

2.2. Implementation of the Tracking Radar

For ACTR to collect different energy from a target that is off the tracking axis, we assume four equally-oblique beams; for PCTR, we assume four beams directed in the identical direction (Fig. 5). The unit vectors of each beam are denoted by $\bar{u}_A$, $\bar{u}_B$, $\bar{u}_C$ and $\bar{u}_D$.

Using the four unit vectors, we constructed an imaginary space composed of the local x-axis, y-axis and the z-axis (= tracking axis) from the global origin (GO) at (0, 0, 0). To express x and y axes, the average of the four unit vectors was set as the local origin (LO) vector

$$\bar{d}_{LO} = \bar{u}_A + \bar{u}_B + \bar{u}_C + \bar{u}_D. \tag{7}$$

Then, for ACTR the x-axis vector $\bar{d}_{LX}$ and y-axis vector $\bar{d}_{LY}$ were constructed as

$$\bar{d}_{LX} = \frac{(\bar{u}_A + \bar{u}_D)}{2} - \bar{d}_{LO}, \quad \bar{d}_{LY} = \frac{(\bar{u}_A + \bar{u}_B)}{2} - \bar{d}_{LO}. \tag{8}$$

For PCTR,

$$\bar{d}_{LX} = \bar{d}_{LO} + \bar{P}_A, \quad \bar{d}_{LY} = \bar{d}_{LO} + \bar{P}_B. \tag{9}$$

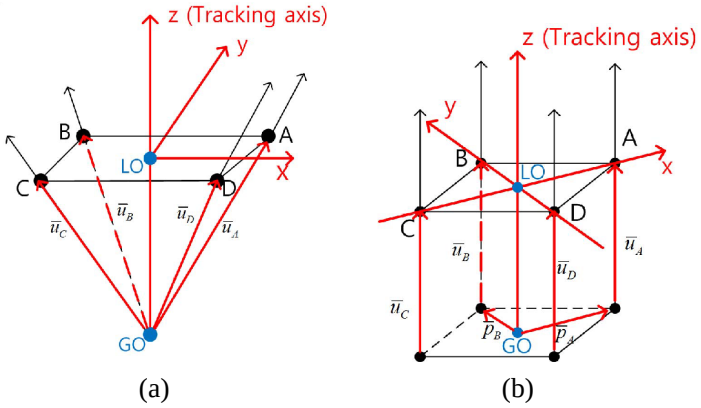

Figure 5. Antenna beam. (a) ACTR. (b) PCTR.

For general use, the unit vectors of the two vectors were constructed using the Euclidean norm of each vector as

$$\bar{u}_{LX} = \frac{\bar{d}_{LX}}{||\bar{d}_{LX}||}, \quad \bar{u}_{LY} = \frac{\bar{d}_{LY}}{||\bar{d}_{LY}||}. \tag{10}$$

In ACTR, when the target is off the tracking axis of ACPR, the tracking axis is moved in the x-y plane until all four antennas collect the same amount of energy. For movement in x-axis, the sums of the power received by beams A and D ($PW_{\text{A-D}}$) and that by beams B and C ($PW_{\text{B-C}}$) are calculated. Then, the amount of movement is obtained by

$$Diff_x = |PW|_{\text{A-D}} - |PW|_{\text{B-C}}. \tag{11}$$

In the same manner, the amount of movement in y-axis is obtained by the two sums of beams A and B ($PW_{\text{A-B}}$) and of beams C and D ($PW_{\text{C-D}}$):

$$Diff_y = |PW|_{\text{A-B}} - |PW|_{\text{C-D}}. \tag{12}$$

Finally, $\bar{d}_{LO}$ in (7) is updated to

$$\bar{d}'_{LO} = \bar{d}_{LO} + \frac{Diff_x}{w}\bar{u}_{LX} + \frac{Diff_y}{w}\bar{u}_{LY}, \tag{13}$$

where w is an appropriate weight that is used to mitigate the increase in tracking error caused by rapid change in the tracking axis. $\bar{u}_A$, $\bar{u}_B$, $\bar{u}_C$ and $\bar{u}_D$ were updated and normalized in the same manner. In implementing PCTR, the same procedure to (10)–(13) was applied by using the geometry in Fig. 5(b) except for the phase difference used to obtain $Diff_x$ and $Diff_y$. Assuming that antenna A is on the positive x-axis and antenna C is on the negative x-axis (Fig. 5(b)) and using (6), $Diff_x$ is obtained by

$$Diff_x = 2\tan^{-1}\left(\frac{|PH_A - PH_C|}{|PH_A + PH_C|}\right), \tag{14}$$

where PH_A and PH_C are the phases of the signal at antennas A and C respectively. For the movement in the y-axis, A and C are replaced by B and D, respectively.

2.3. Signal and Turbine Modeling and Analysis Procedure for the Tracking Radar

The radar signal received by each antenna is generated by the simple radar equation [4–7]. Assuming a target composed of K scatterers represented by the geometric theory of diffraction [8], the total power delivered to the antenna is

$$P_R = \sum_{k=1}^{K} \frac{P_t G^2 \sigma_k}{(4\pi R_k^2)} \exp\left(-j\frac{4\pi}{\lambda}R_k\right), \tag{15}$$

where P_t is the transmitted power, R_k is the distance to scatterer k and σ_k is its RCS, G is the antenna gain and λ is the wavelength.

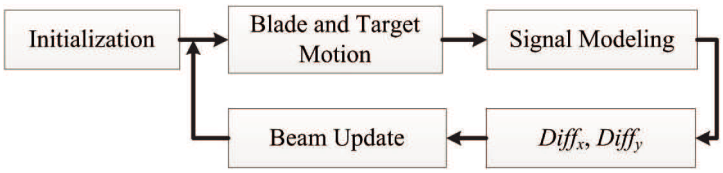

Figure 6. Analysis procedure.

In modeling the motion of the wind turbine, we only consider the blade because the stationary parts have very little influence on the result. As was proposed in [9], the blade motion is assumed to be composed of two components; spinning and nutation. Spinning is the rotation of blades around an axis and nutation is the rotation in a new coordinate formed by the spinning axis and the blade axis. Spinning can be easily modeled using Rodrigues rotation formula, and nutation is modeled by transformation into the new coordinate, sinusoidal rotation and transforming back to the original coordinates [9]. Because the RCS of a blade-like rod can be represented by a single scatterer [3], we assume that each blade has one scatter and that the RCS of the scatter is predicted by the method of PO which is a widely used high-frequency method for RCS prediction [10, 11]. The predicted RCS is used in (16).

In the proposed method (Fig. 6) to analyze the tracking radar, the blade and the target motion are modeled after initialization and the radar signal is collected by (16). Then $Diff_x$ and $Diff_y$ are collected in the local coordinate (Fig. 5) for each tracking radar by using (11), (12) and (15). The beam of each antenna is updated in the same manner. This procedure is repeated until the operation time ends.

2.4. Doppler Analysis of the Wind Farm

For the Doppler analysis, we apply the procedure to analyze the Doppler frequency of L-band radar [9]. The radar signal is modeled by using the chirp signal, and matched filtering is conducted to yield high-resolution signal [12–15]. Then a range bin with the echo signal from the turbine is selected and the short-time Fourier transform [16–19] is conducted to express the time-varying Doppler frequency. Based on the Doppler analysis of a single wind turbine presented in [9], the Doppler analysis on the wind farm was conducted.

3. SIMULATION RESULTS

3.1. Simulation Condition

In simulations, we assumed that the wind farm was located 55 km from the radar, and used a model composed of three blades (Fig. 7(a)); each blade was represented by a single isotropic scatter located at 38.5 m (= blade length) from the center. RCS of each scatterer was set to 10 dBsm by the PO analysis of the three-dimensional (3D) model of the real wind turbine developed by Hyundai Construction (Fig. 7(b)). However, RCSs were varied to study the effect of RCS. To simulate the worst Doppler condition, the spinning axis of each blade which is normal to the unit vector of the wind farm was used. A fast rotation (19 rpm) provided by the turbine maker was used for simulation and for nutation, $\omega_n = 3\pi$ was used with amplitude = 1°.

RCS of a target flying at 250 m/s and 1000 ft altitude was set to 3 dBsm. For the radar system, we used a monostatic system with the pulse repetition frequency (PRF) = 1 kHz, center frequency = 10 GHz, and an antenna with beam = 3.14° and maximum sidelobe level = −26.52 dB. w in (13) was set to 50 for ACTR and 20 for PCTR. Several flight scenarios were simulated by using single and multiple wind turbines and the distance error projected onto the tracking axis was calculated for each scenario to demonstrate the accuracy performance of each radar. In addition, PK was calculated by assuming a Gaussian distribution versus the distance error with the standard deviation = 20 m. For the Doppler analysis, the 38.5-m model with five equally-spaced scatterers (RCS = 10 dB) and 1-MHz bandwidth were used.

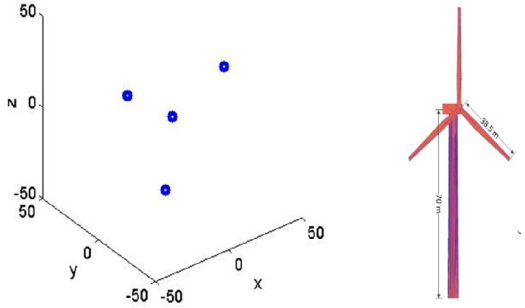

Figure 7. Scatterer model and the real model. (a) Scatterer model. (b) 3D model

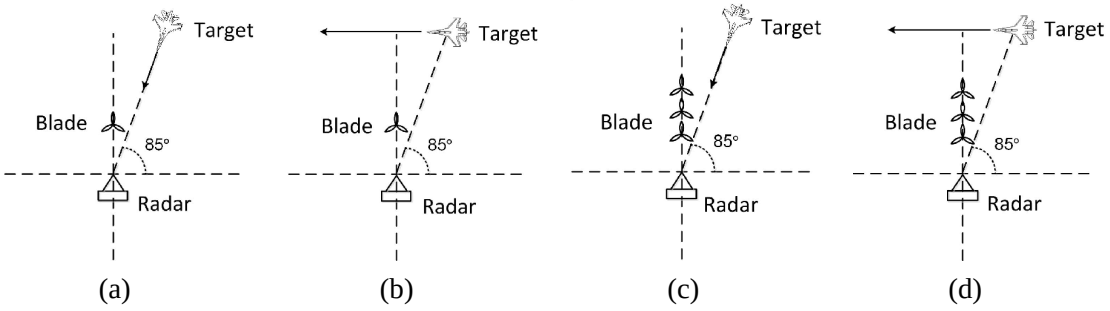

Figure 8. Measurement scenarios. (a) S1 (T1). (b) S1 (T2). (c) S1 (T1). (d) S1 (T2).

3.2. Simulation Results for Various RCS of the Turbine

To study the effect of RCS of each scatterer, two sets of simulations S1 and S2 were performed; in S1, a single turbine was used and in S2, three turbines standing in a line were used (Fig. 8). For S1 and S2, two tests T1 and T2 were performed: in T1 the target closes toward the radar and in T2 the target passes perpendicularly to the line connecting the radar and the blade. For each test, the average PK was calculated for three RCS values of the blade: 0, 5, 10 dBsm.

Both ACTR and PCTR yielded high PK $>$ 96% for RCS = 0; the small difference between ACTR and PCTR was due to the change rate of the beam of each radar. However, at RCS = 5 dBsm, ACTR yielded PK = 0% for both cases because RCS of each scatter larger was than that of the target = 3 dBsm; this difference caused the beam to lock onto the turbine. In contrast, PCTR provided PK $>$ 90%, although they dropped owing to the effect of the large RCS. This is due to the fact that the phase received by the antenna of PCTR was used for tracking and the phase variation of the flying target was much larger than that of the blade.

3.3. Simulation Results for the Wind Farm on PCTR

Because a wind farm is generally composed of several wind turbines, we conducted two sets of simulations by using two types of wind farm F1 and F2 (Fig. 10). Because of the failure of ACTR (Fig. 9), only PCTR was simulated. The flight direction of the target was the same as T1 and T2 in Fig. 8, and RCS values = 0, 5, 15 were used for each test. For in-depth analysis, average, maximum, and minimum values of the distance error and PK were calculated and compared.

The distance error obtained for three RCS values varied significantly (Figs. 11, 12). At RCS = 0, the distance error was close to zero and PK was close to 100% because the target could be regarded as flying without the wind farm (Figs. 11(a) and 12(a)). However, at RCS = 5 and 10, distance error fluctuated between 0 and 4500 m because of the effect of the wind farm (Figs. 11(b) and (c)) and as

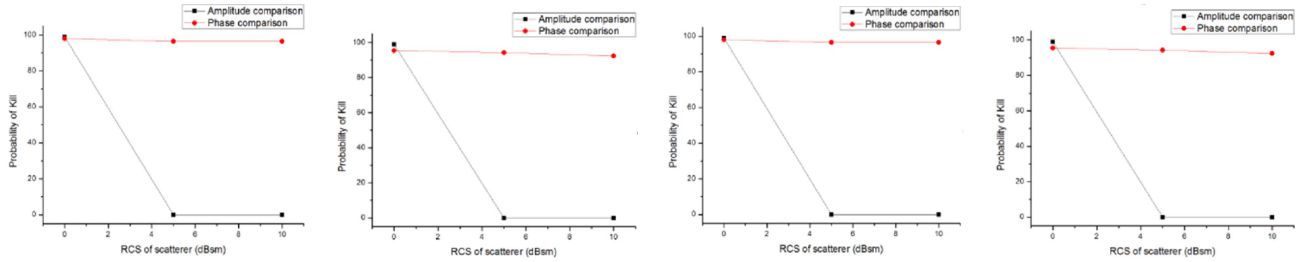

Figure 9. Average probability of kill versus RCS of scatterer for each simulation in Fig. 8. (a) S1 (single). (b) S2 (single). (c) S3 (multiple). (d) S4 (multiple).

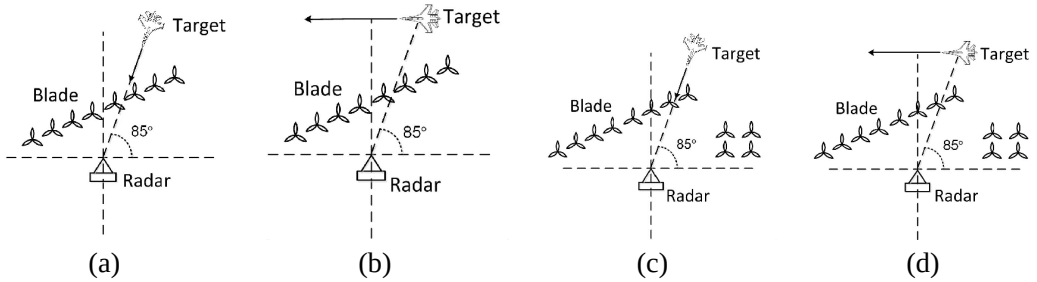

Figure 10. Wind farm and ight scenario used for analysis. (a) F1 (T1). (b) F1 (T2). (c) F1 (T1). (d) F1 (T2).

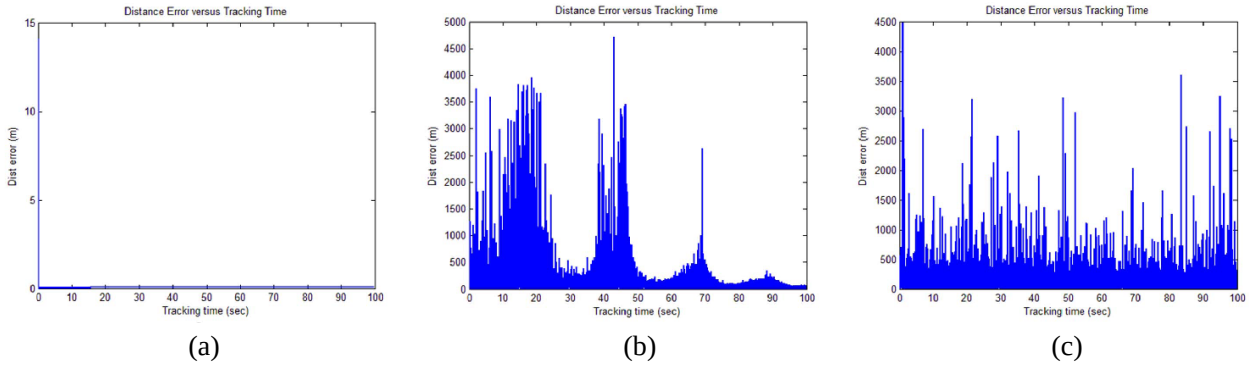

Figure 11. Distance error versus tracking time for the scenario of Fig. 10(a). (a) RCS = 0 dB. (b) RCS = 5 dB. (c) RCS = 10 dB.

a result, PK ranged between 0 and 100% (Figs. 12(b) and (c)). Similar results were obtained for the scenario in Fig. 10(b), so figures are omitted.

The distance error and PK obtained for the scenario of Fig. 10(c) were worse than those for Fig. 10(a) except at RCS = 0 (Figs. 13, 14). At RCS = 0, the distance error and PK were close to zero and 100%, respectively (Figs. 13(a), 14(a)). At RCS = 5 dB, the distance error (Fig. 10(c)) was much more severe than that of Fig. 10(a) because of the influence from the four additional turbines (Fig. 13(b)); distance error was as much as 5000 m and thus PK was very low (Fig. 14(b)). For RCS = 10 dB, the result of Fig. 10(a) was slightly worse than that of Fig. 10(c) (Fig. 13(c) and Fig. 14(c)). Results obtained for Fig. 10(d) were similar to those for Fig. 10(c), so figures are omitted.

The accuracy of the tracking radar degraded significantly because of the interference from the wind farm and degradation was proportional to RCS (Table 1). The average and the maximum distance error increased to as much as 231.9 m (F2, T2, 10-dB RCS) and 4256.0 m (F1, T2, 10-dB RCS), respectively. The average and the minimum PK decreased by as much as 70.0% (F2, T2, 10 dB RCS) and 0.0% (all cases for RCS = 5 and 0 dB).

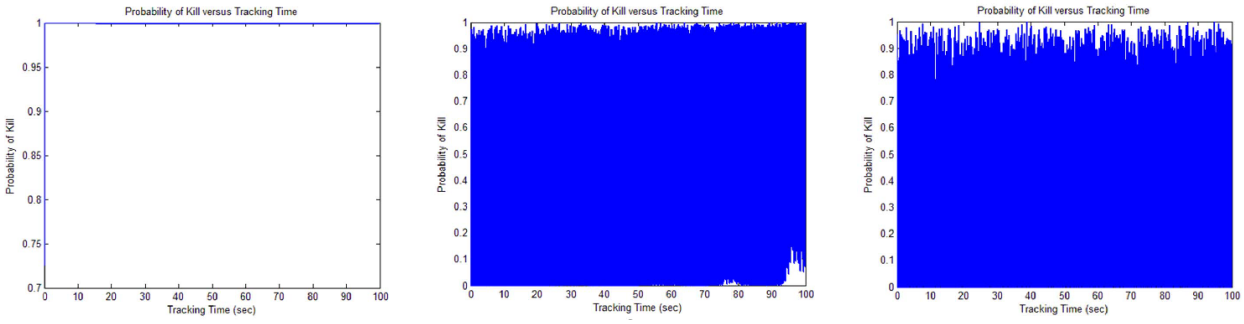

Figure 12. PK versus tracking time for the scenario of Fig. 10(a). (a) RCS = 0 dB. (b) RCS = 5 dB. (c) RCS = 10 dB.

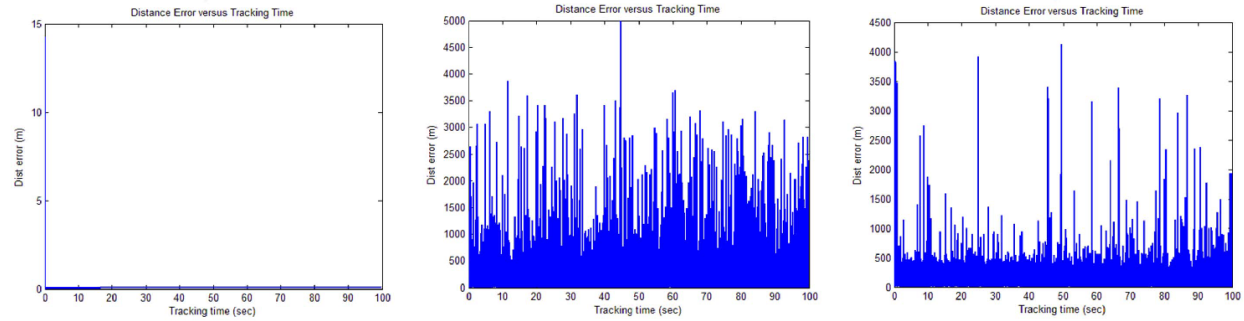

Figure 13. Distance error versus tracking time for the scenario of Fig. 10(c). (a) RCS = 0 dB. (b) RCS = 5 dB. (c) RCS = 10 dB.

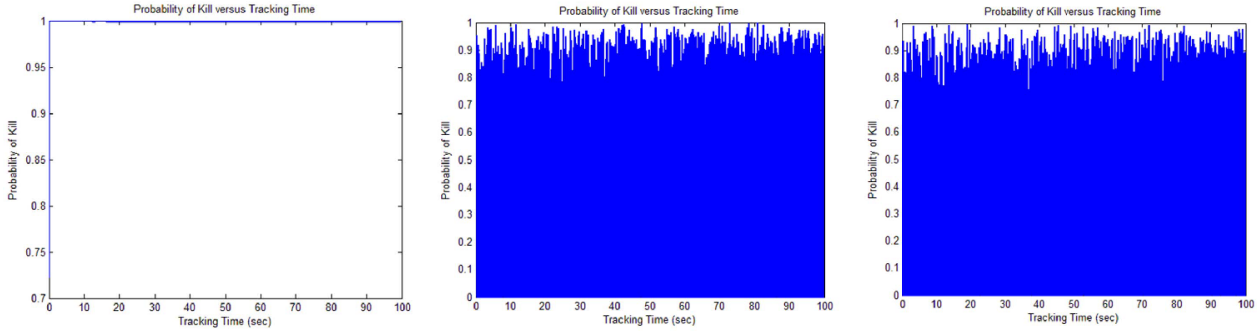

Figure 14. PK versus tracking time for the scenario of Fig. 10(c). (a) RCS = 0 dB. (b) RCS = 5 dB. (c) RCS = 10 dB.

3.4. Doppler Analysis of the Wind Farm

Assuming that the radar is oriented in 90° to the blade, Doppler analysis was conducted on Wind farm 2 in Fig. 10. Eight range profiles (RPs) were formed in order of the distance projected onto the radar line of sight. Because the distances from the first blade on the left to each of the lower two blades on the right are almost equal, the first RP includes the RPs of all three blades (Fig. 15(a)). Therefore, the time-frequency Doppler curves obtained from the first RP overlapped (Fig. 15(b)). The maximum Doppler amplitude was 10 kHz and this corresponds to velocity = 150 m/s, which is the speed of a general military helicopter. Therefore, estimation of helicopter velocity can be seriously impeded by the interference from the wind farm.

Table 1. Simulation results for all scenarios.

Farm	Test	Blade RCS (dB)	Distance error(m)			PK(%)		
			Average	Max	Min	Average	Max	Min
F1	T1	0	0.1	14.1	0.0	99.9	100.0	72.5
		5	102.2	4722.0	0.1	79.2	99.9	0.0
		10	116.8	4483.0	0.1	72.3	99.8	0.0
	T2	0	2.39	18.6	2.0	95.2	96.1	64.1
		5	171.3	4192.7	0.1	77.1	99.9	0.0
		10	198.9	4256.0	0.0	74.3	99.9	0.0
F2	T1	0	0.1	14.2	0.0	99.9	100.0	72.2
		5	209.5	4996.1	0.0	73.6	100.0	0.0
		10	166.3	4122.3	0.2	72.6	100.0	0.0
	T2	0	2.4	17.7	1.8	95.2	96.4	65.9
		5	231.6	4146.3	0.3	72.5	99.4	0.0
		10	231.9	4211.5	0.2	70.0	95.5	0.0

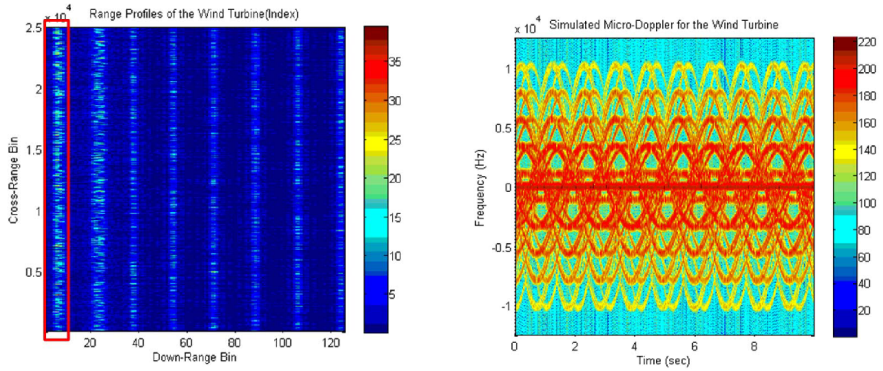

(a) (b)

Figure 15. Doppler analysis of the wind farm 2. (a) RP. (b) Doppler frequency.

4. CONCLUSION

We proposed a method to analyze how the accuracy of a tracking radar system is affected by radar reflections from a wind farm composed of several wind turbines. A real wind turbine model constructed by a Korean wind turbine was used to ensure accurate analysis. In simulations using a single turbine for various RCS values, ACTR was very vulnerable to the large energy reflected from the wind turbine and as a result, PK was close to 0%. However, PCTR tracked the target properly with PK $> 90\%$ because of the large speed of the target. In simulations to study the effect of the two wind farms using two flight scenarios for various RCS values, PK obtained by PCTR decreased by $> 20\%$ because of the large average distance error. In the analysis of the Doppler frequency, 10 kHz was obtained; this corresponds to the speed of a military helicopter speed, so interference from the wind farm could impede detection of such a helicopter. These results show that measures to mitigate the loss of detection accuracy are required. Possible solutions include signal processing to filter out the signal from the wind farm; data sharing among several radars positioned in different locations; and active electrically-scanned array radar that enables high-resolution beam steering.

Based on the procedure proposed in this paper, various wind farms which are under construction along the coast line of Korea will be analyzed and the result will be provided to the Korean Ministry of National Defense as a reference for military operation using the tracking radar. In addition, because many other types of radars that operate along the Korean coast can be affected by the wind farm, we are analyzing the effect of wind farms on these radars. In addition, further research to remove the negative effect by the wind farm is in progress by using the multi-static radar signal, and a new signal

processing technique is being studied. The improved result will be published soon in open literature.

ACKNOWLEDGMENT

This research was supported by Basic Science Research Program through the National Research Foundation of Korea (NRF) funded by the Ministry of Education, Science and Technology (2012R1A1A1002047).

REFERENCES

1. Park, H.-G., K. K. Park, H.-T. Kim, and K.-T. Kim, "Improvement of RCS prediction using modified angular division algorithm," *Progress In Electromagnetics Research*, Vol. 123, 105–121, 2012.
2. Costa, F., S. Genovesi, and A. Monorchio, "A frequency selective absorbing ground plane for low-RCS microstrip antenna arrays," *Progress In Electromagnetics Research*, Vol. 126, 317–332, 2012.
3. Mahafza, B. R., *Radar Systems Analysis and Design Using MATLAB*, Chapman & Hall/CRC, 2000.
4. Cumming, I. G. and F. H. Wong, *Digital Processing of Synthetic Aperture Radar Data*, Artech House, 2005.
5. Skolnik, M., *Introduction to Radar Systems*, MgGRAW-Hill, 2001.
6. Skolnik, M., *Radar Handbook*, MgGRAW-Hill, 1990.
7. Richards, M. A., J. A. Sheer, and W. A. Holm, *Principles of Modern Radar*, SciTech Publishing, 2010.
8. Potter, L. C., D. M. Chiang, R. Carriere, and M. J. Gerry, "A GTD-based parametric model for radar scattering," *IEEE Transactions on Antennas and Propagation*, Vol. 43, No. 10, 1058–1067, Oct. 1995.
9. Jung, J.-H., U. Lee, S.-H. Kim, and S.-H. Park, "Micro-Doppler analysis of Korean offshore wind turbine on the L-band radar," *Progress In Electromagnetics Research*, Vol. 143, 87–104, 2013.
10. Park, S. H., K. K. Park, J. H. Jung, H. T. Kim, and K. T. Kim, "Construction of training database based on high frequency RCS prediction method for ATR," *Journal of Electromagnetic Waves and Applications*, Vol. 22, Nos. 5–6, 693–703, 2008.
11. Klement, D., J. Preissner, and V. Stein, "Special problems in applying the physical optics method for backscatter computations of complicated objects," *IEEE Transactions on Antennas and Propagation*, Vol. 36, No. 2, 228–237, Feb. 1988.
12. Jung, J. H. and S. H. Park, "Efficient classification of low-resolution range profiles of automobiles using a combination of useful features," *Progress In Electromagnetics Research*, Vol. 139, 373–387, 2013.
13. Park, S. H., "Automatic recognition of targets in formation using range profiles," *Journal of Electromagnetic Waves and Applications*, Vol. 26, Nos. 14–15, 2059–2069, 2012.
14. Kim, K. T., J. I. Park, and S. H. Park, "Motion compensation for squint mode spotlight SAR imaging using efficient 2D interpolation," *Progress In Electromagnetics Research*, Vol. 128, 503–518, 2012.
15. Park, S.-H., J. -H. Lee, and K.-T. Kim, "Performance analysis of the scenario-based construction method for real target ISAR recognition," *Progress In Electromagnetics Research*, Vol. 128, 137–151, 2012.
16. Qian, S., *Introduction to Time-frequency and Wavelet Transforms*, Prentice Hall, 2001.
17. Qian, S. and D. Chen, *Joint Time-frequency Analysis*, Prentice Hall, 1998.
18. Chen, V. C., *The Micro-Doppler Effect in Radar*, Artech House, 2011.
19. Han, S.-K., H.-T. Kim, S.-H. Park, and K.-T. Kim, "Efficient radar target recognition using a combination of range profile and time-frequency analysis," *Progress In Electromagnetics Research*, Vol. 108, 131–140, 2010.